

RESEARCH ARTICLE | MAY 30 2017

## A coarse-grain molecular dynamics study of oil–water interfaces in the presence of silica nanoparticles and nonionic surfactants

Parul Katiyar; Jayant K. Singh



*J. Chem. Phys.* 146, 204702 (2017)

<https://doi.org/10.1063/1.4984073>



View  
Online



Export  
Citation

CrossMark

### Articles You May Be Interested In

Aggregation In Heavy Water Micellar Dilute Solutions Of Three Nonionic Classic Surfactants: C10E7 AND C12E7 And C14E7 Study By SANS Method

*AIP Conference Proceedings* (January 2010)

Oil-water interfaces with surfactants: A systematic approach to determine coarse-grained model parameters

*J. Chem. Phys.* (May 2018)

Simulation of surfactant adsorption at liquid–liquid interface: What we may expect from soft-core models?

*J. Chem. Phys.* (September 2022)



Time to get excited.  
Lock-in Amplifiers – from DC to 8.5 GHz



[Find out more](#)



Zurich  
Instruments

# A coarse-grain molecular dynamics study of oil–water interfaces in the presence of silica nanoparticles and nonionic surfactants

Parul Katiyar and Jayant K. Singh<sup>a)</sup>

Department of Chemical Engineering, Indian Institute of Technology Kanpur, Kanpur 208016, India

(Received 16 February 2017; accepted 11 May 2017; published online 30 May 2017)

In this work, we have studied the effect of hydrophilic silica nanoparticles (NPs), in the presence of nonionic surfactants (Triethylene glycol monododecyl ether and Tween 20), on the oil–water (n-octane–water, n-dodecane–water and n-hexadecane–water) interfacial tensions (IFTs) at 300 K, using coarse-grained molecular dynamics simulations based on the MARTINI force field. Simulation results indicate that silica NPs solely do not affect the IFT. However, the silica NPs may or may not increase the IFT of oil–water containing nonionic surfactant, depending on the tendency of the surfactant to adsorb on the surface of NPs. The adsorption occurs due to the formation of hydrogen bonds, and adsorption increases with a decrease in pH, as seen in experimental studies. In this work, we found that the oil–water IFT increases with an increasing amount of adsorption of the surfactant on NPs. At a fixed amount of adsorption of the surfactant on NPs, the IFT behavior is indifferent to the change in concentration of NPs. However, the IFT decreases with an increase in surfactant concentration. We present a detailed analysis of the density profile and intrinsic width of the interface. The IFT behavior is found to correlate extremely well with the intrinsic width of the interface. The current study provides an explanation for the increase in IFT observed in a recent experiment [N. R. Biswal *et al.*, *J. Phys. Chem. B* **120**, 7265–7274 (2016)] for various types of NPs and nonionic surfactant systems. Published by AIP Publishing. [<http://dx.doi.org/10.1063/1.4984073>]

## I. INTRODUCTION

Reducing the interfacial tension (IFT) between two immiscible fluids using the external agents, such as nanoparticles (NPs) and surfactants, enables the fluids to find applications in detergents, emulsions, cosmetics, pharmaceutical, foams, coating industry, and petroleum industry.<sup>1</sup> Thus, numerous works have been conducted to understand the behavior of the IFT in the presence of NPs and surfactants. Several studies have already focused on the IFT of n-alkane–water systems<sup>2–8</sup> and oil–water systems containing surfactants,<sup>9,10</sup> protein,<sup>11</sup> amphiphilic molecules,<sup>12</sup> and surfactin molecules.<sup>13</sup> From these studies, it is clear that adding the surfactant modifies the interfacial properties such that it always reduces the IFT of fluid–fluid interfaces.<sup>14,15</sup>

Distinct from surfactants, adding NPs can affect the IFT in all possible ways. For example, silica NPs have no effect on the IFT of air–water, TCE–water,<sup>16</sup> decane–water,<sup>17</sup> and vegetable oil–water<sup>18</sup> systems. Similarly, hydrophobic bacteria,<sup>19</sup> hydrocarbon NPs,<sup>20</sup> and ZnO NPs<sup>21,22</sup> also have no effect on the oil–water IFT. However, hydrophilic alumina NPs<sup>23</sup> and magnetite NPs<sup>24</sup> increase the oil–water IFT. On the contrary, addition of hydrophobic alumina NPs<sup>23</sup> decreases the oil–water IFT. The above suggests a strong influence of the NP–fluid interaction strength on the IFT.

The influence of NPs along with surfactants has also been studied in view of widespread industrial applications, such as mineral flotation, particle stability, detergency, deinking, and

several others.<sup>25,26</sup> It has been reported that adding NPs along with the surfactant may or may not affect the IFT of the oil–water system. For example, adding hydrocarbon NPs<sup>27</sup> has no effect on the IFT and interfacial thickness of the water–trichloroethylene system containing Sodium dodecyl sulfate (SDS) surfactant. Similarly, hydrophilic silica NPs also show no influence on IFT, when added to air–water and dodecane–water systems containing the zwitterionic surfactant (caprylamidopropyl betaine).<sup>28</sup> On the other hand, various other reports indicate that NPs can help surfactants in reducing the IFT of the oil–water interface. For example, magnetite<sup>24</sup> and silica<sup>15,16,29</sup> NPs increase the efficiency of SDS in reducing the IFT of the oil–water interface. In the first case, magnetite NPs weaken the repulsive interactions between SDS molecules, while in the later study, the electrostatic repulsions between silica NPs and SDS promote the diffusion of SDS towards the interface and thus reduce the IFT. ZnO NPs also increase the efficiency of CTAB<sup>21</sup> and gemini surfactants (12-3-12 and 14-3-14)<sup>22</sup> in decreasing the IFT, due to the synergistic effect.

There are also instances when an increase in the IFT is observed with the addition of NPs to the oil–water system containing surfactants. For example, when silica NPs are added to the air/oil–water system having CTAB, the electrostatic attraction between CTAB and silica NPs causes most of the CTAB to adsorb on the NPs leaving very less amount of free surfactant molecules at the interface,<sup>29–32</sup> leading to an increase in the IFT. Similarly surface tension of sodium dodecyl benzene sulfonate solution also increases with the addition of single-walled carbon nanotubes (SWCNTs), due to the adsorption of the surfactant on the carbon nanotubes (CNTs) to stabilize them in the aqueous solution.<sup>33</sup>

<sup>a)</sup> Author to whom correspondence should be addressed: jayantks@iitk.ac.in. Tel.: 91-512-259 6141. Fax: 91-512-259 0104.

While the aforementioned studies are based on ionic surfactants, in applications like cosmetics, food products, and pharmaceuticals, nonionic surfactants<sup>14,16,18</sup> are preferred with nanoparticles to stabilize the emulsions. Ma *et al.*<sup>16</sup> carried out a study at a pH of 10 and observed no change in IFT with the addition of negatively charged silica NPs (13 nm, 10 wt. %) to the trichloroethylene–water system, containing nonionic (Triton X-100, C<sub>8</sub>E<sub>4</sub>, C<sub>12</sub>E<sub>4</sub>, C<sub>14</sub>E<sub>4</sub>) surfactants. This behavior is attributed to the weak affinity between the nonionic surfactant and the NPs at the specified pH. However, a similar study was carried out by Pichot *et al.*<sup>18</sup> at a pH of 2, where adding silica NPs (12 nm, 1% aerosol) increased the IFT of the oil–water system having a low concentration of nonionic surfactants (Tween 60 and sodium caseinate), which is contradictory to the result of Ma *et al.*<sup>16</sup> Interestingly, the results of Pichot *et al.*<sup>18</sup> are in agreement with the recent works of Biswal *et al.*<sup>15,34</sup> Biswal *et al.*<sup>15,34</sup> observed an increase in the IFT on the addition of SiO<sub>2</sub>/ZnO/TiO<sub>2</sub> NPs to n-hexane/n-heptane/n-decane/toluene–water systems, having nonionic surfactants (Triton X-100 and Tween 20). These results clearly contradict the results of Ma *et al.*<sup>16</sup> However the different behaviors observed for the IFT in the presence of silica NPs and nonionic surfactants by various authors have not been explained in the literature.

In addition to the experimental studies, molecular dynamic (MD) simulations have also been carried out to study the effect of hydrophobic NPs on the heptane–water system containing nonionic surfactants (C<sub>12</sub>E<sub>3</sub>).<sup>14</sup> The results show a decrease in the IFT with the addition of NPs, as the NPs accompany surfactants at the interface. To gain further insight into the interactions between NPs and nonionic surfactants, self-organization of n-alkyl poly(ethylene oxide), C<sub>m</sub>E<sub>n</sub> aqueous surfactants at a planar graphite-like surface has been studied.<sup>35</sup> In addition, adsorption of anionic (SDS) and nonionic (C<sub>12</sub>E<sub>6</sub>) surfactants on the silica surface has also been studied with varying degrees of hydroxylation.<sup>25</sup> The discrete charge distribution on the substrate surface appears to dictate both surfactant adsorption and aggregate morphology.

It is evident based on the aforementioned literature that the behavior of NPs along with ionic surfactants is well understood, as it is mainly governed by the electrostatic interactions. On the other hand, a complex behavior is associated with nonionic surfactants, which varies due to several parameters such as pH and degree of hydroxylation. This complex behavior allows NPs to behave differently in different environments. Consequently, at some instances for the same system, the IFT of oil–water increases in the presence of NPs with nonionic surfactants. On the other hand, for other cases, no change in the IFT of oil–water is observed in the presence of NPs. Thus, the key objectivity of this work is to understand the cause for a different behavior in the IFT upon the addition of NPs to oil–nonionic surfactant solutions.

Coarse-grained (CG) molecular dynamic simulations based on the MARTINI model have been carried out as the calculation of the IFT of oil–water system containing NPs and surfactants; using the atomistic model is computationally very expensive. The MARTINI force field has been reported for calculating the surface tension of different MARTINI water

models such as standard<sup>36</sup> and polarizable.<sup>37</sup> The MARTINI model has also been applied to study the IFT of liquid–liquid interfaces.<sup>36,38,39</sup> Marrink *et al.*<sup>36</sup> showed that the calculated dodecane–vapor/water IFT values are in good agreement with the experimental values. Neyt *et al.*<sup>38</sup> also calculated the IFT of liquid–liquid interfaces, altered using salt and alcohol. Another work by the same group is the one in which Ndao *et al.*<sup>39</sup> studied the dependence of the IFT on temperature and alkane chain length. In this work, we have studied the effect of silica NPs and nonionic surfactant on the IFT of the oil–water interface. In order to understand the behavior in the experimental works, we have also investigated the behavior of NPs with free and adsorbed surfactants, and its consequence on the IFT values. The rest of the article is organized as follows: Simulation details are described in Sec. II, Sec. III discusses the results, and finally conclusions are contained in Sec. IV.

## II. MODEL AND SIMULATION DETAILS

The process of coarse graining involves reducing the degree of freedom by representing the group of atoms by a bead. In this work, we have used different molecules coarse grained based on the MARTINI model.<sup>36</sup> In general, the MARTINI model maps four heavy atoms (excluding hydrogen) to a single bead, while for structures containing ring, two or three atoms are mapped to a bead. There are four main types of interaction sites: polar (P), non-polar (N), apolar (C), and charged (Q). Each main type is further divided into subtypes depending on its hydrogen bonding capabilities as donor (d), acceptor (a), both (da), and none (0), or by a number denoting a degree of polarity from high (5) to low (1).

The total interaction energy in the MARTINI force field is a contribution from non-bonded, bonded, and electrostatic interactions. Non-bonded interactions are given by the Lennard–Jones (LJ) 12-6 potential energy function as defined in Eq. (1), where  $\epsilon$ ,  $\sigma$ , and  $r$  are the interaction strength, the closest distance of approach, and the distance between two particles, respectively. Equation (2) represents the truncated and shifted function to make Eq. (1) continuous at the cut-off ( $r_c$ ), and the expression  $U_{LJ\_shift}(r)$  is zero for  $r > r_c$ . The LJ interactions between the second nearest neighbors are also included in the simulations,

$$U_{LJ}(r) = 4\epsilon \left[ \left(\frac{\sigma}{r}\right)^{12} - \left(\frac{\sigma}{r}\right)^6 \right], \quad (1)$$

$$U_{LJ\_shift}(r) = U_{LJ}(r) - U_{LJ}(r_c) \text{ for } r \leq r_c. \quad (2)$$

Bonded interactions are defined for bonds and angles connecting the CG beads. Bonds are described by weak harmonic potential as

$$U_{bond}(r) = K_{bond}(r - r_0)^2, \quad (3)$$

where  $K_{bond}$  is the force constant and  $r_0$  is the equilibrium bond distance. The LJ interaction is excluded between bonded particles. The angle between the connected beads is defined using the harmonic potential of cosine type as

$$U_{angle}(\theta) = K_{angle}[\cos(\theta) - \cos(\theta_0)]^2, \quad (4)$$

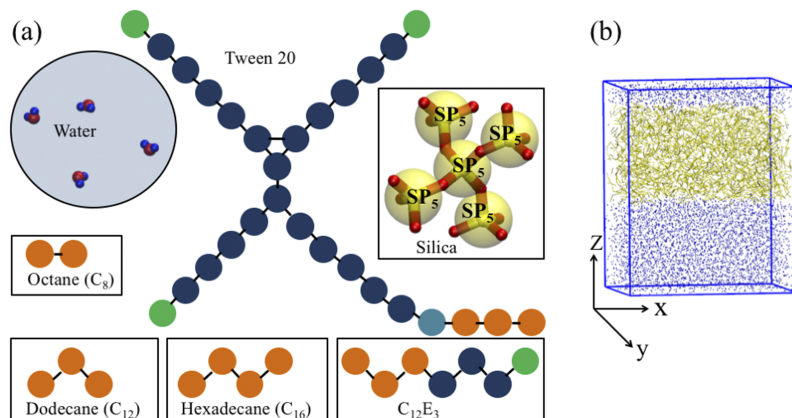


FIG. 1. (a) A cartoon showing various molecules used in simulations in their coarse-grained form. Four water molecules are represented as one bead. Brown, green, blue, and light blue represent C<sub>1</sub>, SP<sub>n</sub>, SP<sub>0</sub>, and COCO beads, respectively. Each SiO<sub>2</sub> group of silica NP is represented by a SP<sub>5</sub> bead. (b) A snapshot showing the simulation box used for the study, having two phases, oil and water, and two interfaces.

where  $K_{angle}$  is the force constant and  $\theta_0$  is the equilibrium bond angle. All the molecules in this study are considered without any charges, so there is no contribution of the electrostatic interactions to the total interaction energy.

The coarse-grained beads for different molecules used in this study are illustrated in Fig. 1. In the MARTINI force field,<sup>36</sup> four water molecules are represented by a single bead having type P<sub>4</sub> (non-polarizable water model), and 10% antifreeze particles of type BP<sub>4</sub> are added to P<sub>4</sub> beads in order to avoid freezing of CG water between 280 and 300 K. BP<sub>4</sub> and P<sub>4</sub> beads have different self interaction parameters, but are similar in interaction with all other beads. Nonionic surfactant C<sub>12</sub>E<sub>3</sub> is modeled the same as used by Rossi *et al.*<sup>40</sup> The coarse-grained Tween 20 structure is as per the method adopted by Amani *et al.*<sup>41</sup> for polysorbate 80, and the interaction parameters are taken from the work of Rossi *et al.*<sup>40</sup> The silica NP is made from crystalline cristobalite silica. A sphere of 30 Å diameter is cut from the crystal. All the oxygen atoms are removed and the silicon atoms are replaced by a CG bead of type SP<sub>5</sub>. The CG silica NP obtained is a spherical cluster of SP<sub>5</sub> beads having a diameter of 30 Å. The non-bonded interaction parameters of an individual bead of a silica NP are taken from the work of Pérez-Sánchez *et al.*,<sup>42</sup> where they have parameterised charged cyclic silica oligomers by SQ<sub>da</sub> bead. In this work, we have modeled a silica nanoparticle as an uncharged cyclic silica oligomer. In another work, Pérez-Sánchez *et al.*<sup>43</sup> reported that the same non-bonded interaction parameters can be used for both charged and uncharged beads. Thus, we have considered an uncharged bead (SP<sub>5</sub>) in place of a charged bead (SQ<sub>da</sub>), both having the same self- and cross-interaction parameters. The NPs are kept rigid during the simulations. The interaction parameters used in simulations are described in Tables I and II. Simulations are performed using LAMMPS package,<sup>44</sup> in NPTA ensemble,<sup>38</sup> where the number of particles, pressure, temperature, and area of the interface are kept constant during the simulations. The velocity-Verlet algorithm is used for integrating the equations of motion. For simulations involving C<sub>12</sub>E<sub>3</sub> molecule, a time step of 20 fs<sup>40</sup> is used, while in simulations not involving C<sub>12</sub>E<sub>3</sub>, 30 fs is used. The temperature is maintained at 300 K and pressure at 1 atm using the Nosé-Hoover thermostat and barostat with the damping parameters of 1.0 ps and 5.0 ps, respectively. The simulation box is a rectangular parallelepiped in which the box length in the x and y directions

(L<sub>x</sub> and L<sub>y</sub>) is kept fixed at 150 Å. The box length (L<sub>z</sub>) in the z direction fluctuates to maintain the equilibrium density of different phases present in the system. This is done by using the barostat only in the z direction. Periodic boundary conditions are applied in all the directions, due to which two interfaces are present in the system. The cut-off value,  $r_c = 13$  Å, is used along with the truncated and shifted potential function in place of  $r_c = 12$  Å and the standard shift function of GROMACS<sup>45</sup> as used by Marrink *et al.*<sup>36</sup> Oils such as octane (10 000 molecules), dodecane (6667 molecules), and hexadecane (5000 molecules) are used along with water (20 000 beads) in the simulations. The simulation box contains oil and water phases, to which either NPs or surfactant or a mixture of both is added, to study the effect of changing concentration of NPs and surfactants. Grafted NPs used in this study are made by attaching the hydrophilic end of the surfactant (C<sub>12</sub>E<sub>3</sub>) chain to a hydrophilic silica NP surface and freezing the attached bead with the NPs, while rest of the beads of the surfactant are flexible. The grafting is done following a similar mechanism as anticipated in the experiments<sup>46</sup> and it is different from the work of Ranatunga *et al.*,<sup>14</sup> where they have grafted the hydrophobic part of the surfactant to a hydrophobic NP surface. Grafted NPs are prepared using Packmol package.<sup>47</sup> All the snapshots are generated using VMD, a molecular visualization program.<sup>48</sup>

TABLE I. Non-bonded interaction parameters.

Molecule	Bead type	$\epsilon$ (kcal/mol)	$\sigma$ (Å)
Water	P <sub>4</sub> -P <sub>4</sub>	1.195 03	4.7
Antifreeze	BP <sub>4</sub> -BP <sub>4</sub>	1.195 03	4.7
Water-antifreeze	P <sub>4</sub> -BP <sub>4</sub>	1.338 43	5.7
Oil, C <sub>12</sub> E <sub>3</sub> , Tween 20	C <sub>1</sub> -C <sub>1</sub>	0.836 52	4.7
Oil, C <sub>12</sub> E <sub>3</sub> , Tween 20-water	P <sub>4</sub> /BP <sub>4</sub> -C <sub>1</sub>	0.478 00	4.7
NP	SP <sub>5</sub> -SP <sub>5</sub>	1.003 8	4.3
NP-Water	SP <sub>5</sub> -P <sub>4</sub> /BP <sub>4</sub>	1.338 43	4.7
NP-Oil, C <sub>12</sub> E <sub>3</sub> , Tween 20	SP <sub>5</sub> -C <sub>1</sub>	0.478 00	4.7
C <sub>12</sub> E <sub>3</sub> , Tween 20	SP <sub>0</sub> -SP <sub>0</sub> /SP <sub>n</sub> /COCO	0.806 64	4.3
C <sub>12</sub> E <sub>3</sub> , Tween 20	SP <sub>n</sub> -COCO	0.806 64	4.3
C <sub>12</sub> E <sub>3</sub> , Tween 20	SP <sub>n</sub> -SP <sub>n</sub>	0.896 2	4.3
Oil-C <sub>12</sub> E <sub>3</sub> , Tween 20	C <sub>1</sub> -SP <sub>0</sub> /SP <sub>n</sub> /COCO	0.645 31	4.7
Water-C <sub>12</sub> E <sub>3</sub> , Tween 20	P <sub>4</sub> /BP <sub>4</sub> -SP <sub>0</sub> /SP <sub>n</sub> /COCO	1.015 7	4.7
Tween 20	COCO-COCO	0.836 52	4.3
NP-C <sub>12</sub> E <sub>3</sub> , Tween 20	SP <sub>5</sub> -SP <sub>0</sub> /SP <sub>n</sub> /COCO	0.950 04	4.3

TABLE II. Bonded interaction parameters.

Bonds		
Bond type	$K_{bond}$ [kcal/(mol Å <sup>2</sup> )]	$r_o$ (Å)
C <sub>1</sub> –C <sub>1</sub>	1.493	4.7
C <sub>1</sub> –SP <sub>0</sub>	5.975	4.1
SP <sub>0</sub> –SP <sub>0</sub>	8.365	3.3
SP <sub>0</sub> –SP <sub>n</sub>	8.365	2.8
SP <sub>0</sub> –COCO	1.493	4.3
COCO–C <sub>1</sub>	1.493	4.7
Angles		
Angle type	$K_{angle}$ (kcal/mol)	$\theta_0$ (deg)
C <sub>1</sub> –C <sub>1</sub> –C <sub>1</sub>	2.9875	180
C <sub>1</sub> –C <sub>1</sub> –SP <sub>0</sub>	2.9875	180
C <sub>1</sub> –SP <sub>0</sub> –SP <sub>0</sub>	2.9875	180
SP <sub>0</sub> –SP <sub>0</sub> –SP <sub>0</sub>	23.9006	135
SP <sub>0</sub> –SP <sub>0</sub> –SP <sub>0</sub> (ring)	23.9006	120
SP <sub>0</sub> –SP <sub>0</sub> –SP <sub>n</sub>	2.9875	140
SP <sub>0</sub> –SP <sub>0</sub> –COCO	2.9875	180
SP <sub>0</sub> –COCO–C <sub>1</sub>	2.9875	180
COCO–C <sub>1</sub> –C <sub>1</sub>	2.9875	180

The IFT ( $\gamma$ ) of the oil–water interface is calculated using the following expression:<sup>49,50</sup>

$$\gamma = \frac{1}{2} \left\langle L_z \left( P_{zz} - \frac{P_{xx} + P_{yy}}{2} \right) \right\rangle, \quad (5)$$

where  $L_z$  is the box length in the z direction and  $P_{xx}$ ,  $P_{yy}$ , and  $P_{zz}$  are the pressures in the x, y, and z directions, respectively. A factor of  $1/2$  in Eq. (5) comes from the fact that there are two oil–water interfaces present in the system. In this work, we have calculated the pressure component using the virial method.<sup>51</sup> The simulations are run for 900 ns equilibration. The production run is varied from 300 ns to 900 ns depending on the NPs concentration. The average value of the IFT is based on the block averages of the production run.

The interfacial width is obtained by fitting the density profiles of oil and water as obtained from our simulations to the following equations:<sup>52</sup>

$$\rho_1(z) = \frac{1}{2} \rho_1 - \frac{1}{2} \rho_1 \operatorname{erf} \left( \frac{z - \langle h_1 \rangle}{\sqrt{2} w_c} \right), \quad (6)$$

$$\rho_2(z) = \frac{1}{2} \rho_2 + \frac{1}{2} \rho_2 \operatorname{erf} \left( \frac{z - \langle h_2 \rangle}{\sqrt{2} w_c} \right), \quad (7)$$

where  $\rho_1$  and  $\rho_2$  are the densities of two liquids 1 and 2, here oil and water.  $\langle h_1 \rangle$  and  $\langle h_2 \rangle$  are the average positions of the interface for liquids 1 and 2, respectively. Equations (6) and (7) fitted to the density profile data yield the value of intrinsic width,  $w_0 = |h_1 - h_2|$  and the width due to thermal fluctuations,  $w_c$ .

### III. RESULTS AND DISCUSSIONS

The surface tension/interfacial tension calculated using the MARTINI force field deviates from the experimental values.<sup>39</sup> First, we have performed few simulations to compare

TABLE III. Surface tension/interfacial tension,  $\gamma$  (mN/m) of different interfaces using coarse-grained simulations at two different cut-off values, 12 and 13 Å at a temperature of 300 K, and their comparison with experiments and reference simulations.

T (K)	$r_c = 13$ Å $\gamma$	$r_c = 12$ Å $\gamma$	Reference simulation <sup>39</sup>	
			$\gamma_{exp.}$	$\gamma_{sim.}$
Water–vacuum				
300	$39.60 \pm 0.28$	$35.39 \pm 0.16$	72.86 (293 K)	30 (293 K)
Octane–vacuum				
300	$26.42 \pm 0.26$	$23.95 \pm 0.33$	21.62 (293 K)	...
Hexadecane–vacuum				
300	$31.93 \pm 0.28$	$29.23 \pm 0.35$	27.05	...
Octane–water				
300	$48.71 \pm 0.37$	$44.21 \pm 0.28$	51.2	$41.1 \pm 0.8$
Dodecane–water				
300	$51.20 \pm 0.35$	$46.66 \pm 0.30$	52.8	$42.6 \pm 1.0$
Hexadecane–water				
300	$52.88 \pm 0.36$	$48.18 \pm 0.25$	53.3	$43.2 \pm 1.0$

our results with the literature based on the MARTINI model and experimental values. Table III summarizes these results. The surface tension of water using the MARTINI model is significantly lower than that of the experimental value, and with increasing cut-off ( $r_c$ ) distance, viz., 12, 13, 14, 15, 20, and 25 Å, the surface tension values are found to be 35.39, 39.60, 42.96, 45.74, 53.95, and 57.89 mN/m, respectively, reaching closer to the experimental value with an increasing  $r_c$  value. For oils such as octane (C<sub>8</sub>) and hexadecane (C<sub>16</sub>), the surface tension is overestimated compared to the experimental values. It is noted that the surface tension is closest to the experimental value at  $r_c = 12$  Å and deviates more at 13 Å. On the other hand, for liquid–liquid systems, the calculated IFT of C<sub>8</sub>–water, C<sub>12</sub>–water, and C<sub>16</sub>–water is underestimated as compared to the experimental values. The IFT increases with the increase in  $r_c$  from 12 to 13 Å, and at  $r_c = 13$  Å, the IFT is close to the experimental value. The values obtained in this work are an improvement over the reference simulation values<sup>39</sup> obtained using the MARTINI force field with  $r_c = 12$  Å and the standard shift function of GROMACS.<sup>45</sup> For example, in the work of Ndao *et al.*,<sup>39</sup> the reported deviation of the oil–water IFT from the experiments is ~20%. In another work by Neyt *et al.*,<sup>38</sup> the deviation of the oil–water IFT reaches ~27%, while in the present study, the deviation reduces to less than 6% from the experiments. Apart from IFT, we also looked into the bulk density of liquids, and they are summarized in Table IV. It is noted that the deviation in densities is more as compared to that of reference simulations.<sup>39</sup> Furthermore, the increase in  $r_c$  value further increases the deviation in the density value for oils. In this work, our focus is on the liquid–liquid interfacial tension, and thus, we have fixed a cut-off distance  $r_c = 13$  Å in the entire study, as  $r_c = 13$  Å provides IFT values for oil–water closer to the experimental values without much deviation in densities from the known values of the MARTINI model. The MARTINI model also holds good for the variation of IFT with temperature and alkyl chain length of oil. In Fig. 2, the IFT decreases with an increase in the temperature

TABLE IV. Bulk densities,  $\rho$  (g/cm<sup>3</sup>) of liquids used in simulations at 300 K, and their comparison with experiments and reference simulations.

System	$r_c = 13\text{\AA}$ $\rho$	$r_c = 12\text{\AA}$ $\rho$	Experiments <sup>39</sup> $\rho_{\text{expt.}}$	Reference simulation <sup>39</sup> $\rho_{\text{sim.}}$
Octane	$0.814 \pm 0.002$	$0.804 \pm 0.002$	0.700	0.799
Water	$0.931 \pm 0.002$	$0.921 \pm 0.002$	0.997	1.052
Hexadecane	$0.845 \pm 0.002$	$0.836 \pm 0.002$	0.770	0.832

and increases with an increase in the alkyl chain length. The slope of  $\gamma$  vs. T plot gives a value of  $-0.13 \text{ mN}/(\text{m K})$  for both oil–water systems, which is in agreement with the literature,<sup>39</sup> but differs slightly from the experimental slope of  $-0.10 \text{ mN}/(\text{m K})$ . The above analysis concludes that the IFT of oil–water interfaces can be reproduced reasonably well using the MARTINI force field at different temperatures. The system size chosen in this study is large enough such that the oil–water IFT values reported in the entire study show negligible difference when the interfacial area of each interface is increased by 4 times. Thus, the obtained IFT values have no system size effect.

### A. Effect of hydrophilic silica NPs on oil–water IFT

Oil–water systems have been studied using the MARTINI force field in the past,<sup>38,39</sup> but the effect of NPs on the IFT has not been studied much. Figure 3 shows the IFT of the oil–water system in the presence of hydrophilic silica NPs. The IFT values are unaffected by the addition of NPs and are nearly constant with an increase in the concentration of NPs. The constant value of IFT is attributed to the hydrophilic nature of NPs, which promotes them to stay completely in bulk water as shown in a snapshot in Fig. 3. The observed behavior of IFT is in agreement with the previous experiments done with silica<sup>15–18,34</sup> and other NPs<sup>20–22</sup> in oil–water systems. All the oil–water systems such as C<sub>16</sub>–water, C<sub>12</sub>–water, and C<sub>8</sub>–water behave in the similar manner in our simulations.

We have also looked into the density profiles of the C<sub>16</sub>–water system in the presence of NPs. Figure 4(a) shows the density profile at 2.15 vol. % of NPs. It is evident from the figure that two well-developed phases, viz., for water and oil, are observed, where NPs are found to immerse in the water

phase. Figure 4(b) shows the effect of changing NPs concentration on the oil and water density profiles. It is evident from the figure that no change in the density profiles of C<sub>16</sub> and water is observed with increasing concentration of NPs. The density profile shows a clear picture of the interfacial width. The interfacial width reduces with an increase in the sharpness of the density profile. A lower interfacial width suggests a higher IFT and vice versa.<sup>6</sup> The overlapping density profiles (or constant interfacial width) suggest an indifferent behavior of the IFT, which is well supported by Fig. 3. This is also in line with the work of Luo *et al.*<sup>20</sup> where the constant interfacial width of the oil–water system is reported with the addition of NPs.

### B. Effect of nonionic surfactant and silica NPs on oil–water IFT

In this section, we extend our study to understand the effect of NPs on the water–oil system containing nonionic surfactant. Figure 5(a) presents the IFT values of C<sub>8</sub>–water as a function of the interfacial area per surfactant (triethylene glycol monododecyl ether, C<sub>12</sub>E<sub>3</sub>) molecule for two cases, with and without NPs. The results of C<sub>8</sub>–water with C<sub>12</sub>E<sub>3</sub>, without NPs, are consistent with the results of Ranatunga *et al.*,<sup>14</sup> where they observed a similar behavior with C<sub>12</sub>E<sub>3</sub> without NPs at the heptane–water interface. It is clear that the IFT of the oil–water interface increases with an increase in the interfacial area per surfactant (equivalent of decreasing concentration). The behavior is similar in nature for the case of the C<sub>16</sub>–water system as shown in Fig. 5(b). It is evident from Fig. 5(a) and Fig. 5(b) that the same amount of surfactant has more impact on the IFT of C<sub>16</sub>–water as compared to the C<sub>8</sub>–water interface. A larger decrease in IFT is observed for oil with a longer alkyl chain length in the presence of surfactant. Fig. 5 also displays the combined effect of both surfactants (C<sub>12</sub>E<sub>3</sub>)

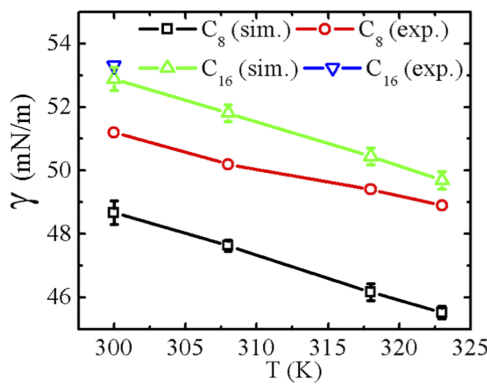


FIG. 2. The variation of IFT ( $\gamma$ ) with temperature (T) for different oil–water systems and their comparison with experimental values.

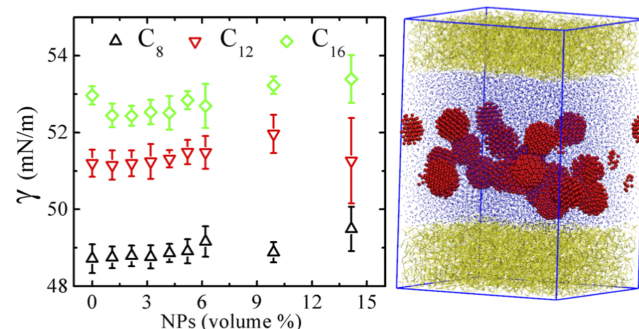


FIG. 3. IFT ( $\gamma$ ) values for various oil–water systems at different silica NPs concentrations. The snapshot shows the location of silica NPs in the C<sub>16</sub>–water system. Blue, red, and yellow represent water, NPs, and oil, respectively.

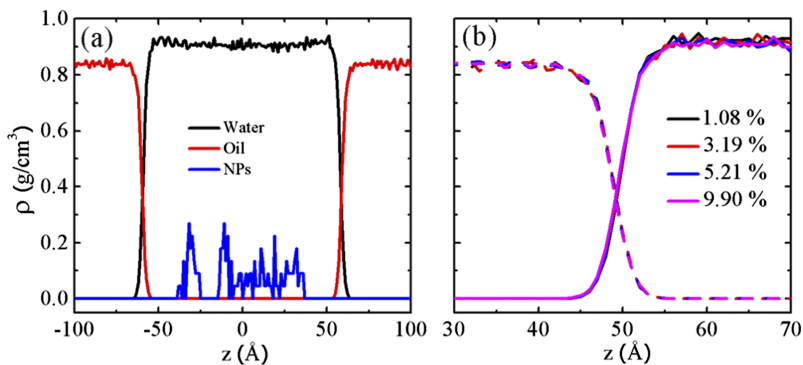


FIG. 4. (a) The density profile ( $\rho$ ) for the  $C_{16}$ -water silica NPs system, at 2.15 vol. % NPs. (b)  $C_{16}$  and water density profiles at different NPs vol. %. Different colored lines represent different vol. % of NPs in the system. Dashed lines indicate the oil phase, while solid lines represent water.

and NPs on IFT. Red circles in Fig. 5 show the IFT for 3.19 vol. % of NPs at different surfactant concentrations. The presence of NPs along with the surfactant shows the same value of IFT as that of the surfactant alone. Thus the IFT behavior with surfactant concentration is indifferent to the presence of NPs. Similar results are reported for silica NPs and nonionic surfactants in the literature by Ma *et al.* at a pH of 10.<sup>16</sup>

Figure 6(a) shows the density profiles for  $C_{16}$ -water, NPs (3.19 vol. %), and  $C_{12}E_3$  system, and it is observed that the surfactant resides at the interface with their head group in water, tail in oil, and NPs in bulk water. The increasing concentration of surfactant has a broadening effect on the density profile of the oil–water interface as shown in Fig. 6(b) and hence an increase in the interfacial width. As the width of interface increases, the IFT decreases.<sup>6</sup> The density profiles of oil–water and  $C_{12}E_3$  systems with and without NPs are found to overlap due to the negligible effect of NPs (figure is not shown).

Further to ensure that NPs do not affect the IFT, we varied the concentration of NPs for a fixed concentration of  $C_{12}E_3$  (150 and 450 Å<sup>2</sup> per surfactant), and the IFT values are shown in Fig. 6(c). The IFT values show negligible increase with increasing NPs concentration, for both the concentrations of  $C_{12}E_3$ . The density profile for 150 Å<sup>2</sup> per  $C_{12}E_3$  molecule at 2.15, 4.21, and 14.16 vol. % of NPs is shown in Fig. 6(d). It is evident from the figure that at a fixed surfactant concentration and with varying NPs' concentrations, all the density profiles coincide with each other indicating that the interfacial width and hence IFT are the same. Thus, no change is observed in the IFT with the addition of silica NPs to the oil–water system containing nonionic surfactants.

There are several studies, as summarized in the Introduction, which shows an increase in IFT with the addition of NPs to the oil–water system having nonionic surfactants. One of those studies includes a nonionic surfactant, Tween 20.<sup>15</sup> In order to understand the generality of the effect of NPs on the oil–water system, containing nonionic surfactants, we extend our study to include Tween 20. We performed separate simulations with Tween 20 in oil–water in the presence of silica NPs, and NPs are found to cause no effect on the IFT of the oil–water Tween 20 system, as shown in Fig. 7. It is clear that our molecular dynamic simulation results are in disagreement with the experimental results of Pichot *et al.*<sup>18</sup> and Biswal *et al.*<sup>15,34</sup> Thus, we now attempt to understand the cause for the increase in IFT in the aforementioned experimental studies. Biswal *et al.*<sup>15</sup> postulated two reasons for the increase in IFT for the oil–water Tween 20 system in the presence of NPs. First, NPs hinder the transport of surfactant from bulk to the interface, and/or NPs displace the surfactant molecules from the interface to the bulk. Second, surfactant molecules get adsorbed on the surface of NPs, thus reducing the amount of surfactant at the interface. The first postulate is ruled out in this study because silica NPs are hydrophilic NPs, and thus, NPs do not come to the oil–water interface. The second postulate, i.e., adsorption of surfactants on the NP surface, can be a reason for such a behavior.

Penfold *et al.*<sup>46</sup> have mentioned in their work that “The dominant interaction between nonionic surfactants and the hydrophilic surface of silica is due to hydrogen bonding of the ether oxygen of the ethylene oxide group and the surface –OH groups.” This statement leads to an understanding that hydrogen bonding is responsible for the adsorption of surfactants on the NPs. According to Penfold *et al.*,<sup>46</sup> silica has an isoelectric

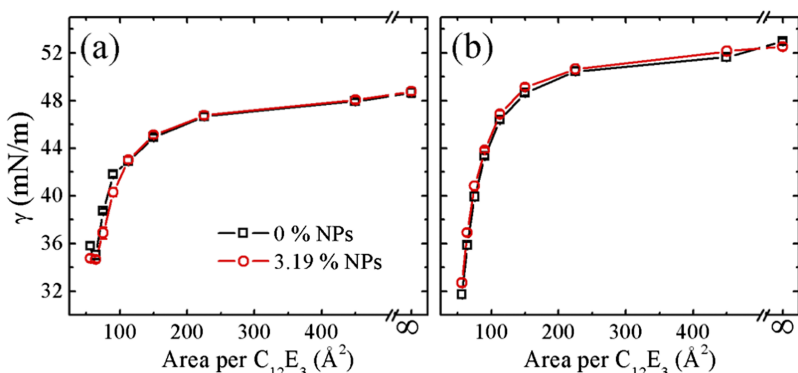


FIG. 5. The IFT of (a) octane–water and (b) hexadecane–water in the presence of surfactants and NPs (vol. %), for varying interfacial area per  $C_{12}E_3$  molecule.

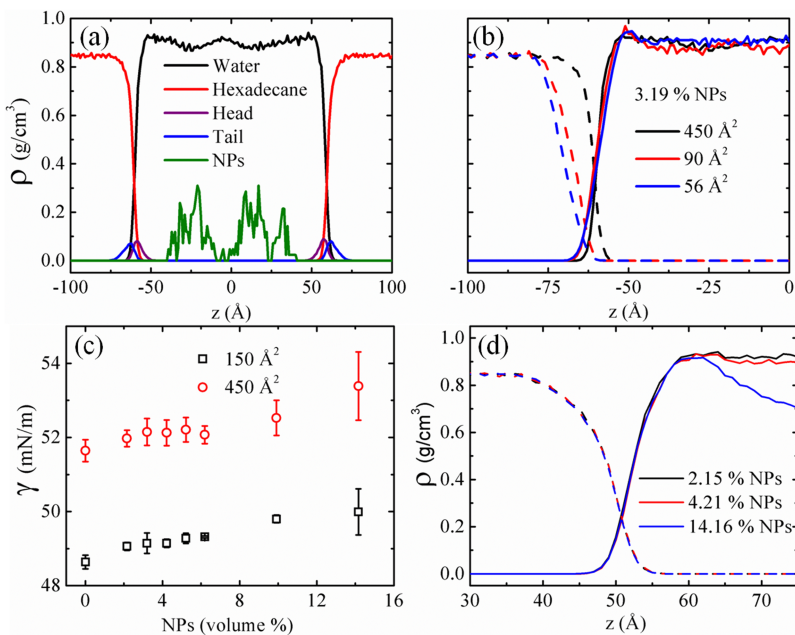


FIG. 6. (a) The density profile of C<sub>16</sub>-water, NPs, and C<sub>12</sub>E<sub>3</sub> system, containing 3.19 vol. % NPs, and surfactant concentration corresponding to an interfacial area of 450 Å<sup>2</sup> per C<sub>12</sub>E<sub>3</sub>, (b) C<sub>16</sub> and water density profiles at the same NPs concentration as (a), and for several values of area per C<sub>12</sub>E<sub>3</sub>. (c) The variation of IFT with NPs concentration at a fixed surfactant concentration of 150 Å<sup>2</sup> (black) and 450 Å<sup>2</sup> (red) per C<sub>12</sub>E<sub>3</sub> molecule in C<sub>16</sub>-water. (d) The density profiles of C<sub>16</sub> and water at 150 Å<sup>2</sup> per C<sub>12</sub>E<sub>3</sub> and 2.15, 4.21, and 14.16 vol. % of NPs. Dashed lines indicate the oil phase, while solid lines represent water.

point at a pH in the range 1–2. Above pH 2.0, the surface is net negatively charged, and it begins to dissolve at pH more than 9.0. The adsorption of the nonionic surfactant is significantly greater at pH 2.4 than that at pH 7.0, and desorption occurs at pH more than 9. This shows that the adsorption of nonionic surfactants on the silica surface is highly pH dependent. As the pH reduces, within the range of acidic pH, there is a higher concentration of H<sup>+</sup> ions in the solution and so the dissociation of silanol (−SiOH) groups into −SiO<sup>−</sup> and H<sup>+</sup> is less. Consequently, a large number of silanol groups are available on silica NPs to form hydrogen bonds with the ether oxygen of ethylene oxide group present in the nonionic surfactant and hence increase in the adsorption of the surfactant on NPs. As the pH increases in the alkaline range, the concentration of hydroxyl ions in the solution also increases, and so a very large fraction of silanol (−SiOH) group on the surface of silica NPs dissociates to give H<sup>+</sup> ions and itself acquires a negative charge. As the number of silanol groups decreases, there are less number of sites available for the formation of hydrogen bonds, and thus the adsorption keeps on decreasing with an increase in pH. In other words, reducing pH will reduce the surface charge

density and will increase the density of hydroxyl groups on the surface, which will enhance the surfactant adsorption on NPs. When pH is more than 7, almost all the −SiOH groups are dissociated and hence negligible adsorption should be observed. In summary, as the pH increases the degree of ionization of silica NPs increases,<sup>53</sup> and hence the adsorption decreases.

### C. Effect of nonionic surfactant: Free and adsorbed on NPs

From the discussions in Sec. III B, it is clear that hydrogen bonding leads to the adsorption of nonionic surfactant on silica NPs and as a consequence increases the IFT of the oil–water, surfactant system. The studies showing an increase in the IFT with the addition of silica NPs to the oil–water system containing nonionic surfactants were either carried out at a pH of 2<sup>16</sup> or without maintaining any fixed pH.<sup>15,34</sup> At a pH of 2, there would be an adsorption of surfactants on NPs. In case when no fixed pH is maintained, for systems containing silica NPs in water, it is found that pH varies in the range from 5 to 7.<sup>54</sup> Thus, the pH of the studies by Biswal *et al.*<sup>15,33</sup> lies in the range such that the adsorption of nonionic surfactants on silica NPs would occur. This strongly suggests that all the studies, which showed an increase in the IFT, had surfactants adsorbed on the surface of NPs. The results presented above in this study did not observe any adsorption of surfactant on the NPs. Consequently no change in IFT on the addition of silica NPs to the oil–surfactant solution is seen. The MARTINI model is unable to capture the hydrogen bonding and hence cannot be used directly to predict the experimental results of Biswal *et al.*<sup>15,34</sup>

Since the model could not capture the adsorption behavior of the nonionic surfactant on silica NPs and its effect on the IFT, we considered the surfactant directly tethered on NPs to understand the effect of adsorption on the IFT. Here, we have tethered the silica NPs with the surfactant (C<sub>12</sub>E<sub>3</sub>) chains and call them as grafted NPs. The effect of increasing

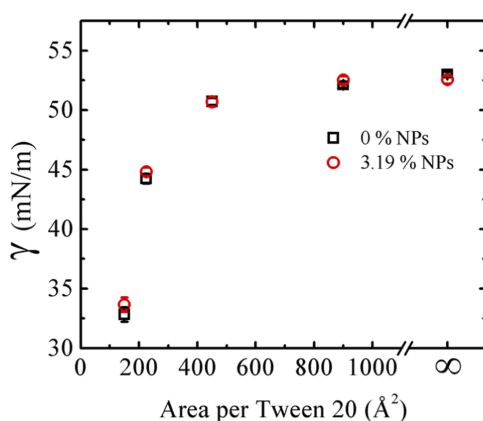


FIG. 7. The variation of the IFT with the concentration of Tween 20, for C<sub>16</sub>-water system in the presence of Tween 20 and NPs (vol. %).

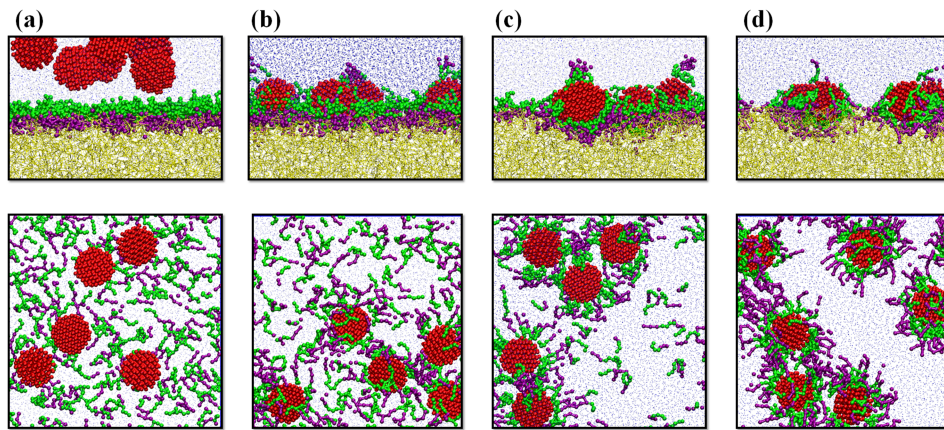


FIG. 8. The representative snapshots of simulations for 5.21 vol. % of NPs and  $112.5 \text{ \AA}^2$  interfacial area per  $\text{C}_{12}\text{E}_3$  molecule in the  $\text{C}_{16}$ –water system at a different amount of surfactants adsorbed at (a) 0%, (b) 50%, (c) 75%, and (d) 100% on NPs. The top row shows the side view of the system displaying only one interface and the bottom row shows the top view of the system. In the snapshot, red, green, purple, yellow, and blue represent NPs, hydrophilic part of surfactant, hydrophobic part of surfactant,  $\text{C}_{16}$ , and water, respectively.

adsorption is studied by keeping total number of  $\text{C}_{12}\text{E}_3$  molecules fixed and increasing the number of adsorbed surfactants.  $\text{C}_{12}\text{E}_3$  molecules are either tethered to the NP surface or kept in free form depending on the percentage of adsorbed surfactant. In case of 0% adsorption, all the surfactant molecules are free from the NPs surface or rather they do not adsorb on the NP surface (corresponding to high pH  $\sim 10$ ). For 25% adsorption, 25% of total surfactant molecules are adsorbed on the NPs surface and rest 75% are free (unadsorbed). For 100% adsorption, all the surfactant chains are adsorbed on the NPs. In the simulations, we have assumed that the adsorbed surfactants are equally distributed on all the NPs present in the system. Figure 8 shows the snapshots with the side view and top view for a different amount of surfactants adsorbed on NPs. In Fig. 8(a) there is no adsorption (0% adsorption), and from the side view it is evident that only the surfactant molecules are at the  $\text{C}_{16}$ –water interface, while NPs are away from the interface, in bulk water. From the top view of Fig. 8(a), surfactants are found to disperse uniformly covering the entire interface. In the side view of Figs. 8(b)–8(d), all the NPs

(grafted) move to the interface and stays there, which is different from what is observed for the case of ungrafted NPs [see Fig. 8(a)]. This difference in behavior is due to the fact that the grafted NPs are amphiphilic and surface active; hence, they move to the interface as opposed to the ungrafted NPs. From the top view of Figs. 8(b)–8(d), with the increasing amount of adsorption of surfactant, the uniformity in the distribution of the free surfactant molecule decreases. Thus, a large area of interface is not covered with the surfactant molecules. Figure 9(a) shows the variation of IFT with the percentage of adsorbed surfactants at a fixed surfactant concentration corresponding to  $112.5 \text{ \AA}^2$  interfacial area per  $\text{C}_{12}\text{E}_3$  molecule, and at various concentrations of NPs. At 0% adsorbed surfactant, the IFT is minimum, and it keeps on increasing as the % of adsorbed surfactant increases to 25%, 50%, 75%, and finally 100%. This indicates that the IFT increases with an increase in the amount of surfactant adsorbed on the NPs. The minimum IFT value is obtained when there is no adsorption. Adsorption reduces the amount of surfactant available to the interface, as also shown in the top view of snapshots in Fig. 8. Hence, the adsorbed surfactant leads to an increase in the IFT. Also, there is a negligible effect of adding different concentrations of NPs on the IFT for a fixed amount of adsorbed surfactant. Figure 9(b) shows the variation of IFT as a function of surfactant concentration, for 2.15 vol. % NPs and different amount of adsorbed surfactants. The increase in IFT with increasing amount of adsorption is also seen for different values of surfactant concentration. It is evident from Fig. 9(b) that the IFT value is maximum for 100% adsorbed case. On the other hand, the effect of the surfactant is maximum in reducing the IFT when there is no adsorption. As the adsorption increases, the effect of surfactant diminishes. In fact, there is almost negligible effect of adding the surfactant for the case of 100% adsorbed surfactant.

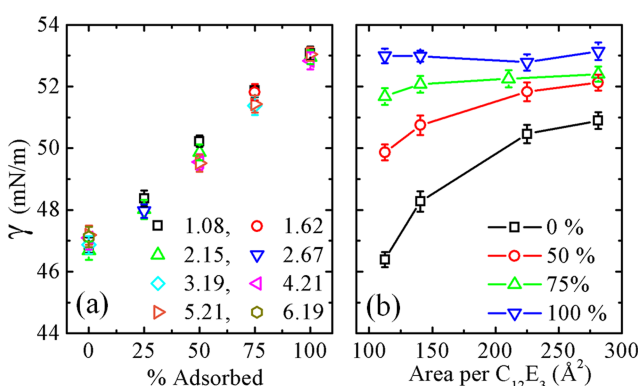
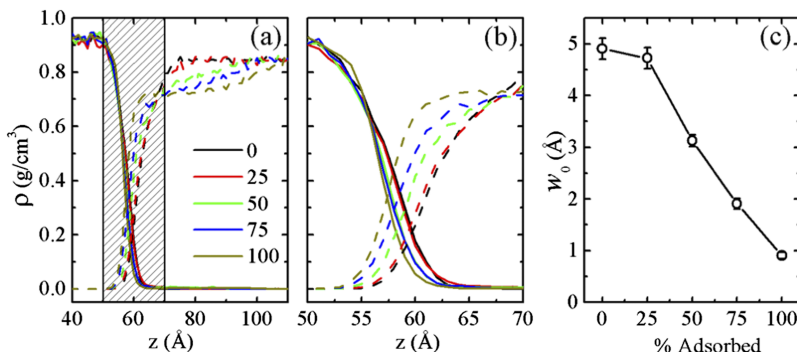


FIG. 9. Variation in the IFT of the  $\text{C}_{16}$ –water interface, (a) with varying percentage of surfactants adsorbed on NPs, for systems containing different volume percentage of NPs, and a fixed amount of surfactant concentration corresponding to  $112.5 \text{ \AA}^2$  interfacial area per  $\text{C}_{12}\text{E}_3$  molecule. Different colored symbols represent different volume percentage of NPs present in the system. (b) Variation in the IFT with the addition of 2.15 vol. % NPs to the  $\text{C}_{16}$ –water system containing different concentrations of  $\text{C}_{12}\text{E}_3$  surfactant. Different colored symbols represent different percentage of surfactants adsorbed on the NPs.

Figure 10(a) shows the density profile for  $\text{C}_{16}$  and water in  $\text{C}_{16}$ –water system with 1.08 vol. % NPs and  $112.5 \text{ \AA}^2$  area per  $\text{C}_{12}\text{E}_3$  molecule, at different percentage of adsorbed surfactants. As the amount of adsorption increases for a fixed vol. % of NPs, the hydrophobic nature of the grafted NPs increases. Therefore, a larger portion of a grafted NP shifts into the oil closer to the interface and away from the bulk water phase. This causes the drop in density values of  $\text{C}_{16}$ , for 50%, 75%, and 100% adsorbed surfactants, before



attaining the bulk density values as clearly seen in Fig. 10(a). The zoomed-in view of the shaded region in Fig. 10(a) is shown in Fig. 10(b), which displays the density profile at the interface. As the percentage of adsorbed surfactant increases, the density profile of  $C_{16}$  and water at the interface becomes sharper. To quantify the density profile, we calculate the intrinsic width of the interface as a function of the adsorbed surfactant in Fig. 10(c). It is clear from the figure that with an increase in the adsorption of surfactants on the NPs, the interfacial width decreases. This observation substantiates the results of increase in IFT with increasing adsorbed surfactants. We have demonstrated qualitatively the effect on IFT in the case of no adsorption, adsorption, and increasing adsorption of surfactant on NPs. The results presented in this work qualitatively agree well with experiments. However, the exact amount of adsorption will definitely have an effect on the IFT values, but the behavior is expected to remain the same.

#### IV. CONCLUSIONS

We have investigated the effect of silica NPs and nonionic surfactants on the IFT of the oil–water interface using the MARTINI force field based molecular dynamics simulations. The mechanisms responsible for different behaviors of IFT, on the addition of silica NPs to the oil–water system containing nonionic surfactants, are explained. We observed no effect of silica NPs on the IFT value of the oil–water system containing the nonionic surfactant when NPs and surfactants are free from each other. The adsorption of surfactants on NPs is found to increase the IFT value. The adsorption is due to the formation of hydrogen bonds between the –OH of silanol group on the surface of silica NPs and the ether oxygen of the nonionic surfactant. The hydrogen bonding is affected by the pH of the solution. At high pH, there is a dissociation of –OH of silanol group and hence a decrease in the hydrogen bonding leading to the negligible adsorption of surfactant molecules on silica NPs. As pH decreases, dissociation decreases and so more number of hydrogen bonds are formed, leading to more surfactant adsorption on silica NPs. A systematic study has been done to study the effect of increasing adsorption on the IFT. As the adsorption increases, the IFT also increases. The behavior of IFT with increasing amount of surfactant adsorption is well correlated with interfacial width calculations. Thus, based on our extensive molecular dynamics simulations, we conclude that the adsorption of the nonionic surfactant on silica NPs is the

FIG. 10. (a) The density profile for  $C_{16}$  and water in the  $C_{16}$ –water system containing 1.08 vol. % NPs and 112.5  $\text{\AA}^2$  interfacial area per  $C_{12}\text{E}_3$  molecule. Different colored lines represent different percentage of surfactants adsorbed on NPs. Zoomed-in view of the shaded region in (a) is shown as (b). Dashed lines in the density profile represent oil and solid lines represent water. (c) The intrinsic width of the  $C_{16}$ –water interface as a function of percentage of adsorbed surfactant for the systems as in (a) and (b).

key reason behind the increase in the IFT values of oil–water system.

#### ACKNOWLEDGMENTS

This work is supported by the Council of Scientific and Industrial Research (CSIR), Government of India and Science and Engineering Research Board, Department of Science and Technology (SERB-DST), Government of India. The computational resources are provided by the HPC cluster of the Computer Center (CC), Indian Institute of Technology Kanpur.

- <sup>1</sup>L. L. Schramm, *Surfactants: Fundamentals and Applications in Petroleum Industry* (Cambridge University Press, Cambridge, UK, 2000).
- <sup>2</sup>A. Goebel and K. Lunkenheimer, *Langmuir* **13**, 369 (1997).
- <sup>3</sup>X. HongYan, Z. Zhen, S. HuanQuan, C. XuLong, L. ZhenQuan, S. XinWang, C. XiaoHong, and L. XinHou, *Sci. China: Chem.* **53**, 945 (2010).
- <sup>4</sup>S. Zeppieri, J. Rodríguez, and A. L. L. de Ramos, *J. Chem. Eng. Data* **46**, 1086 (2001).
- <sup>5</sup>P. Than, L. Preziosi, D. D. Joseph, and M. Arney, *J. Colloid Interface Sci.* **124**, 552 (1987).
- <sup>6</sup>J. L. Rivera, C. McCabe, and P. T. Cummings, *Phys. Rev. E* **67**, 011603 (2003).
- <sup>7</sup>A. R. van Buuren, S.-J. Marrink, and H. J. C. Berendsen, *J. Phys. Chem.* **97**, 9206 (1993).
- <sup>8</sup>Y. Fukunishi, T. Tateishi, and M. Suzuki, *J. Colloid Interface Sci.* **180**, 188 (1996).
- <sup>9</sup>J. Amaya, D. Rana, and V. Hornof, *J. Solution Chem.* **31**, 139 (2002).
- <sup>10</sup>B. Smit, P. A. J. Hilbers, K. Esselink, L. A. M. Rupert, N. M. van Os, and A. G. Schlijper, *Nature* **348**, 624 (1990).
- <sup>11</sup>C. J. Beverung, C. J. Radke, and H. W. Blanch, *Biophys. Chem.* **81**, 59 (1999).
- <sup>12</sup>D. L. Cheung, *Langmuir* **28**, 8730 (2012).
- <sup>13</sup>J. P. Nicolas, *Biophys. J.* **85**, 1377 (2003).
- <sup>14</sup>R. J. K. U. Ranatunga, C. T. Nguyen, B. A. Wilson, W. Shinodab, and S. O. Nielsen, *Soft Matter* **7**, 6942 (2011).
- <sup>15</sup>N. R. Biswal, N. Ranger, and J. K. Singh, *J. Phys. Chem. B* **120**, 7265 (2016).
- <sup>16</sup>H. Ma, M. Luo, and L. L. Dai, *Phys. Chem. Chem. Phys.* **10**, 2207 (2008).
- <sup>17</sup>H. Fan, D. E. Resasco, and A. Striolo, *Langmuir* **27**, 5264 (2011).
- <sup>18</sup>R. Pichot, F. Spyropoulos, and I. T. Norton, *J. Colloid Interface Sci.* **377**, 396 (2012).
- <sup>19</sup>Z. Kang, A. Yeung, J. M. Foght, and M. R. Gray, *Colloids Surf., B* **62**, 273 (2008).
- <sup>20</sup>M. Luo, O. A. Mazayar, Q. Zhu, M. W. Vaughn, W. L. Hase, and L. L. Dai, *Langmuir* **22**, 6385 (2006).
- <sup>21</sup>T. F. Moghadam and S. Azizian, *J. Phys. Chem. B* **118**, 1527 (2014).
- <sup>22</sup>T. F. Moghadam, S. Azizian, and S. Wettig, *Phys. Chem. Chem. Phys.* **17**, 7122 (2015).
- <sup>23</sup>J. Saien, F. Moghaddamnia, and H. Bamdad, *J. Chem. Eng. Data* **58**, 436 (2013).
- <sup>24</sup>J. Saien, A. R. Pour, and S. Asadabadi, *J. Chem. Eng. Data* **59**, 1835 (2014).
- <sup>25</sup>N. R. Tummala, L. Shi, and A. Striolo, *J. Colloid Interface Sci.* **362**, 135 (2011).

- <sup>26</sup>A. W. Adamson and A. P. Gast, *Physical Chemistry of Surfaces* (Wiley-Interscience, USA, 1997).
- <sup>27</sup>M. Luo and L. L. Dai, *J. Phys.: Condens. Matter* **19**, 375109 (2007).
- <sup>28</sup>A. J. Worthen, L. M. Foster, J. Dong, J. A. Bollinger, A. H. Peterman, L. E. Pastora, S. L. Bryant, T. M. Truskett, C. W. Bielawski, and K. P. Johnston, *Langmuir* **30**, 984 (2014).
- <sup>29</sup>S. Ahualli, G. R. Iglesias, W. Wachter, M. Dulle, D. Minami, and O. Glatter, *Langmuir* **27**, 9182 (2011).
- <sup>30</sup>F. Ravera, E. Santini, G. Loglio, M. Ferrari, and L. Liggieri, *J. Phys. Chem. B* **110**, 19543 (2006).
- <sup>31</sup>D. C. E. Calzolari, D. Pontoni, M. Deutsch, H. Reichert, and J. Daillant, *Soft Matter* **8**, 11478 (2012).
- <sup>32</sup>P. A. Yazhgur, B. A. Noskov, L. Liggieri, S.-Y. Lin, G. Loglio, R. Millere, and F. Ravera, *Soft Matter* **9**, 3305 (2013).
- <sup>33</sup>R. Kumar and D. Milanova, *Appl. Phys. Lett.* **94**, 073107 (2009).
- <sup>34</sup>N. R. Biswal and J. K. Singh, *RSC Adv.* **6**, 113307 (2016).
- <sup>35</sup>G. Srinivas, S. O. Nielsen, P. B. Moore, and M. L. Klein, *J. Am. Chem. Soc.* **128**, 848 (2006).
- <sup>36</sup>S. J. Marrink, H. J. Risselada, S. Yefimov, D. P. Tieleman, and A. H. d. Vries, *J. Phys. Chem. B* **111**, 7812 (2007).
- <sup>37</sup>S. O. Yesylevskyy, L. V. S. fer, D. Sengupta, and S. J. Marrink, *PLoS Comput. Biol.* **6**, e1000810 (2010).
- <sup>38</sup>J. C. Neyt, A. Wender, V. Lachet, A. Ghoufi, and P. Malfreyt, *J. Chem. Theory Comput.* **10**, 1887 (2014).
- <sup>39</sup>M. Ndao, J. Devemy, A. Ghoufi, and P. Malfreyt, *J. Chem. Theory Comput.* **11**, 3818 (2015).
- <sup>40</sup>G. Rossi, P. F. J. Fuchs, J. Barnoud, and L. Monticelli, *J. Phys. Chem. B* **116**, 14353 (2012).
- <sup>41</sup>A. Amani, P. York, H. de Waard, and J. Anwar, *Soft Matter* **7**, 2900 (2011).
- <sup>42</sup>G. Pérez-Sánchez, S.-C. Chien, J. R. B. Gomes, M. N. D. S. Cordeiro, S. M. Auerbach, P. A. Monson, and M. Jorge, *Chem. Mater.* **28**, 2715 (2016).
- <sup>43</sup>G. Pérez-Sánchez, J. R. B. Gomes, and M. Jorge, *Langmuir* **29**, 2387 (2013).
- <sup>44</sup>S. J. Plimpton, *J. Comput. Phys.* **117**, 1 (1995).
- <sup>45</sup>E. Lindahl, B. Hess, and D. van der Spoel, *J. Mol. Model.* **7**, 306 (2001).
- <sup>46</sup>J. Penfold, E. Staples, and I. Tucker, *Langmuir* **18**, 2967 (2002).
- <sup>47</sup>L. Martínez, R. Andrade, E. G. Birgin, and J. M. Martínez, *J. Comput. Chem.* **30**, 2157 (2009).
- <sup>48</sup>W. Humphrey, A. Dalke, and K. Schulten, *J. Mol. Graphics* **14**, 33 (1996).
- <sup>49</sup>J. K. Singh, D. A. Kofke, and J. R. Errington, *J. Chem. Phys.* **119**, 3405 (2003).
- <sup>50</sup>Y. Zhang, S. E. Feller, B. R. Brooks, and R. W. Pastor, *J. Chem. Phys.* **103**, 10252 (1995).
- <sup>51</sup>M. P. Allen and D. J. Tildesley, *Computer Simulation of Liquids* (Oxford University Press, USA, 1989).
- <sup>52</sup>S. Senapati and M. L. Berkowitz, *Phys. Rev. Lett.* **87**, 176101 (2001).
- <sup>53</sup>F. S. Emami, V. Puddu, R. J. Berry, V. Varshney, S. V. Patwardhan, C. C. Perry, and H. Heinz, *Chem. Mater.* **26**, 2647 (2014).
- <sup>54</sup>P. Katiyar, T. K. Patra, J. K. Singh, D. Sarkar, and A. Pramanik, *Chem. Eng. Sci.* **141**, 293 (2016).